

# Characterization of Orbital Debris Photometric Properties Derived from Laboratory-Based Measurements

H. Cowardin

*ESCG/Jacobs Technology, E-mail: [heather.cowardin@nasa.gov](mailto:heather.cowardin@nasa.gov)*

**P. Seitzer<sup>1</sup>, K. Abercromby<sup>2</sup>, E. Barker<sup>3</sup>, and T. Schildknecht<sup>4</sup>**

*<sup>1</sup>University of Michigan, Department of Astronomy, <sup>2</sup>California Polytechnic State University, Department of Aerospace Engineering, <sup>3</sup>LZ Technology, Inc,*

*<sup>4</sup>Astronomical Institute, University of Bern*

## ABSTRACT

To better characterize and model optical data acquired from ground-based telescopes, the Optical Measurements Center (OMC) at NASA/JSC attempts to emulate illumination conditions seen in space using equipment and techniques that parallel telescopic observations and source-target-sensor orientations. Equipment in the OMC includes a 75-watt Xenon arc lamp, used as a solar simulator; a Santa Barbara Instrument Group CCD camera with standard Johnson/Bessel filters; and a robotic arm, used to simulate an object's position and rotation. The laboratory uses known shapes, materials that are believed to be consistent with the orbital debris population, and three phase angles to best match the lighting conditions of the telescope-based data. The 14 objects studied to-date in the OMC are fragments or materials acquired through ground-tests of scaled-model satellites and rocket bodies, as well as material samples in more or less "flight-ready" condition. All fragments were measured at 10° increments in a full 360° rotation at 6°, 36°, and 68° phase angles.

This paper will investigate published color photometric data for a series of orbital debris targets and compare it to the empirical photometric measurements generated in the OMC. Using the data acquired over specific rotational angles through different filters (B, V, R, I), multiple color indices are acquired. Using these values and their associated lightcurves, the OMC data are compared to observational data obtained from the 1-m telescope of the Astronomical Institute of the University of Bern, and from the 0.9-m telescope operated by the Small- and Medium-Aperture Research Telescope System Consortium and the Curtis-Schmidt 0.6-m Michigan Orbital DEbris Survey Telescope (MODEST), which are both located at the Cerro Tololo Inter-American Observatory. An empirical-based optical characterization on a subset of fragments will be presented to provide preliminary correlations between laboratory-based and telescope-based data in the context of classifying GEO debris objects.

## 1. INTRODUCTION

Optical observations of orbital debris provide time-dependent photometric data that yield lightcurves in multiple bandpasses that aid in material identification and possible periodic orientations. These data can also be used to help identify shapes and optical properties at multiple phase angles. Capitalizing on optical data products and applying them to generate a more complete understanding of orbital space objects is a key objective of NASA's Optical Measurements Program and a primary objective for the creation of the Optical Measurements Center (OMC). The OMC is used to emulate space-based illumination conditions using equipment and techniques that parallel telescopic observations and source-target-sensor orientations.

The following will present the data acquired in the OMC as a function of known shape, size, and material. These three physical parameters are key to understanding the orbital debris environment in more depth. For optical observations, one must rely on spectroscopic or photometric measurements to ascertain an object's material type. Whereas, determination of an object's shape using remote observations is more complicated due to the various light scattering properties each object presents, and therefore, is a subject that requires more study. It is much easier to look at the periodicity of the lightcurve and analyze its structure for rotation.

In order to best simulate the orbital debris population, three main sources were used as test fragments for optical measurements: flight-ready materials, destructive hypervelocity testing (simulating on-orbit collisions), and destructive pressure testing (simulating on-orbit explosions). Laboratory optical characteristics of fragments were

measured, including lightcurve shape, phase angle dependence, and photometric and spectroscopic color indices. These characteristics were then compared with telescopic observations in order to correlate remote and laboratory properties with the intent of ascertaining the intrinsic properties of the observed orbital debris.

## 2. DATA ACQUISITION

The design of the OMC is analogous to a telescope set-up with a light source, target, and observer. A 75-watt, Xenon arc lamp simulates solar illumination through the spectral range of 200 to 2500 nm. The data are acquired through a Santa Barbara Instrument Group CCD camera (1024 x 1536 pixels) with an attached filter wheel that uses the standard astronomical suite of Johnson/Bessell filters: Blue (B), Visible (V), Red (R), and Infrared (I). Spectral measurements are also employed to baseline various material types using a quartz lamp as an illuminator and an Analytical Spectral Device field spectrometer (range from 300-2500 nm). The laboratory phase angle (the vertex angle between source, object, and detector) is capable of obtaining data between 6°- 68° using the maximum space in the optical facility. Specific details on data acquisition can be found in the references [1, 2].

## 3. SAMPLES INVESTIGATED

The investigated samples were chosen to best represent the potential materials in the orbital debris population and are shown in Table 1, together with the corresponding size parameter (characteristic length,  $L_c$ ), mass, and estimated area-to-mass (A/m) values. The  $L_c$  values were calculated using a three-dimensional scanner to reconstruct the object with N-number points and vertices, thus allowing for a more efficient and accurate method for dimensional analysis [3]. The A/m values were calculated using the above-mentioned  $L_c$  and cross-sectional area formulas presented in the NASA 1998 Breakup Model [4]. The objects investigated include a variety of A/m values to best correlate with telescope photometric data. Although the majority of orbital debris are believed to have A/m values < 1.0 m<sup>2</sup>/kg, a new population of debris was detected in GEO in 2005 that exhibited characteristics of objects with higher A/m [5]. High A/m objects possess variable eccentricity and inclination – a characteristic generally resulting from the pronounced effect of solar radiation pressure. Multi-layered insulation (MLI) materials are a common spacecraft material known to have high A/m values (A/m > 2 m<sup>2</sup>/kg), while individual layers of MLI will have much higher A/m values. For comparison, a standard piece of notebook paper (8.5” x 11”) has an A/m ~ 6 m<sup>2</sup>/kg.

Flight-ready materials were obtained from colleagues, the Jet Propulsion Laboratory, and Spectrolab. The Satellite Orbital Debris Characterization Impact Test (SOCIT) 4 [6] and Kyushu University [7] samples both used destructive hypervelocity testing, whereas the European Space Operations Centre (ESOC) 2 test used destructive pressure testing [8].

Table 1. Laboratory samples with respective physical dimensions

ID	Material	Source	Size: $L_c$ (mm)	Mass (kg)	~ A/m (m <sup>2</sup> /kg)
1	Intact MLI	Colleague	57.2	$1.2 \times 10^{-3}$	2.1
2	Layer MLI: Space-facing Kapton	Colleague	58.2	$3.9 \times 10^{-4}$	5.4
3	Layer MLI: Spacecraft-facing Kapton	Colleague	57.6	$5.1 \times 10^{-4}$	4.2
4	Impacted MLI	Kyushu University	83.8	$1.2 \times 10^{-3}$	5
5	Solar panel	Jet Propulsion Laboratory	~60	$5.2 \times 10^{-3}$	0.5
6	Intact Solar cell	Spectrolab	50.1	$4.4 \times 10^{-3}$	0.4
7	Fragment Solar cell	Kyushu University	23.8	$3.1 \times 10^{-4}$	1
8	Aluminum	ESOC2	56.5	$2.6 \times 10^{-3}$	1
9	Glass Fiber Reinforced Plastic	Kyushu University	95.9	$1.7 \times 10^{-2}$	0.4
10	Carbon Fiber Reinforced Plastic	Kyushu University	66.3	$3.2 \times 10^{-3}$	1
11	Nugget – Electronic Potting Material	SOCIT4	17.7	$1.3 \times 10^{-3}$	0.3
12	Electronic Circuit Board	SOCIT4	49.2	$7.1 \times 10^{-3}$	0.2
13	Flake- Aluminum	SOCIT4	22.5	$1.0 \times 10^{-3}$	0.5
14	Potted Electronics	SOCIT4	64.0	$2.2 \times 10^{-2}$	0.2

## 4. LABORATORY MEASUREMENTS

### 4.1. Photometric Color Indices

Laboratory-based photometry, when correlated with telescopic observations, may enable identification of material types. BVRI photometry data have been acquired on various targets averaged over a 360° rotation through one-axis. The relative magnitude calculations are determined using a white reference (spectralon panel); unlike the telescope observations that use the Landolt catalogue to determine the correct color magnitudes. Therefore, the values determined in the OMC will not be identical to telescope magnitudes. Targets were measured at three different phase angles: 6°, 36°, and 68°, to investigate any variances in the light curve characteristics. Initially, the results showed that phase angle does affect the number of peaks each target presents; however, upon further inspection, it is believed that the illumination equipment is causing a bias in the data. This issue is being investigated and the results for phase angle dependence will be presented in the near future. The color index data will be limited to the smallest phase angle in which the least amount of optical illumination error was found. More detailed information on shape analysis and characteristics can be found in *Characterization of Orbital Debris Objects over Optical Wavelengths via Laboratory Measurements* [2].

The uncorrected color index values for all 14 fragments are shown to one digit precision, to the best confidence of the experimental data in Table 2. Several of these objects had a very low signal in the infrared (*I*) wavelengths and showed false lightcurve characteristics. Therefore, the color index with respect to *I* will not be shown for these specific objects. In the material column, if objects were composed of multiple materials, the first material illuminated will be listed first, followed by the second illuminated material, and so on.

In order to compare laboratory photometric data to telescopic data, all the color indices were corrected to solar values, shown in Fig. 1. The legend in Fig. 1 uses short-hand notation to identify the objects, “Cu” for copper-colored, “Al” for aluminized, “space” for space-facing, “S/C” for spacecraft facing, and “K.U.” as the abbreviation for Kyushu University (the only impacted MLI fragment). The copper-colored Kapton (intact MLI, space-facing copper Kapton, spacecraft-facing copper Kapton) all showed color indices much redder than the sun and more reflective in the B-V color index than the sun. The JPL solar panel, which is composed of solar cell, aluminum honeycomb, and carbon fiber reinforced plastic (CFRP), was in the same range as the copper Kapton. The composite, potted electronics were in close range to the solar value, but slightly redder and slightly “greener” (~0.5 each). The fragmented solar cell and green nugget showed much bluer values than the sun, with the green nugget showing the only negative B-R after corrections were applied. Overall, the majority of the objects were very close to solar indices, as shown in Fig. 2 (identical plot to Fig. 1, but rescaled to focus on targets near solar colors).

Table 2. Laboratory samples with respective photometric color indices before solar corrections

ID	Material	Material	B-V	B-R	B-I
1	Intact MLI	Space-facing, spacecraft-facing	+2.0±0.8	+2.9±1.1	+2.5±0.8
2	Layer MLI: Space-facing Kapton	Copper Kapton, Aluminized Kapton	+3.6±1.0, -0.1±0.1	+2.3±1.3, -0.1±0.2	+3.6±1.7, -0.3±0.6
3	Layer MLI: Spacecraft-facing Kapton	Aluminized Kapton, Copper Kapton	-0.1±0.1, +2.1±1.2	-0.1±0.1, +2.8±1.7	-0.8±0.5, +2.8±1.1
4	Impacted MLI	Layers of copper Kapton sandwiched with Mylar and beta cloth substitute	+0.1±0.2	+0.1±0.2	-0.9±1.0
5	Solar panel	Solar cell, aluminum honeycomb interior, CFRP backing	+1.9±0.1	+2.2±0.3	+0.6±1.0
6	Intact Solar cell	Aluminized backing, solar cell	+0.2±0.2	+0.1±0.5	-2.3±1.9
7	Fragment Solar cell	Aluminum back, solar cell	+0.2±0.2	-0.8±1.0	N/A
8	Aluminum	Aluminum alloy	+0.0±0.0	-0.1±0.1	-0.8±0.4
9	Glass Fiber Reinforced Plastic	Glass fiber reinforced plastic	+0.1±0.1	+ 0.1±0.2	N/A
10	Carbon Fiber Reinforced Plastic	Carbon fiber reinforced plastic	+0.1±0.1	+0.1±0.0	N/A
11	Nugget - Potting Material	Plastic potting material	+0.4±0.1	-1.3±0.8	N/A
12	Electronic Circuit Board	Plastic back side, electronics	+0.3±0.1	+0.1±0.3	-3.0±0.5
13	Flake- Aluminum	Possible aluminum with unknown surface contaminants	+0.0±0.0	+0.1±0.0	-0.6±0.4
14	Potted Electronics	Metals and plastics	+0.3±0.1	+0.5±0.1	+0.5±0.1

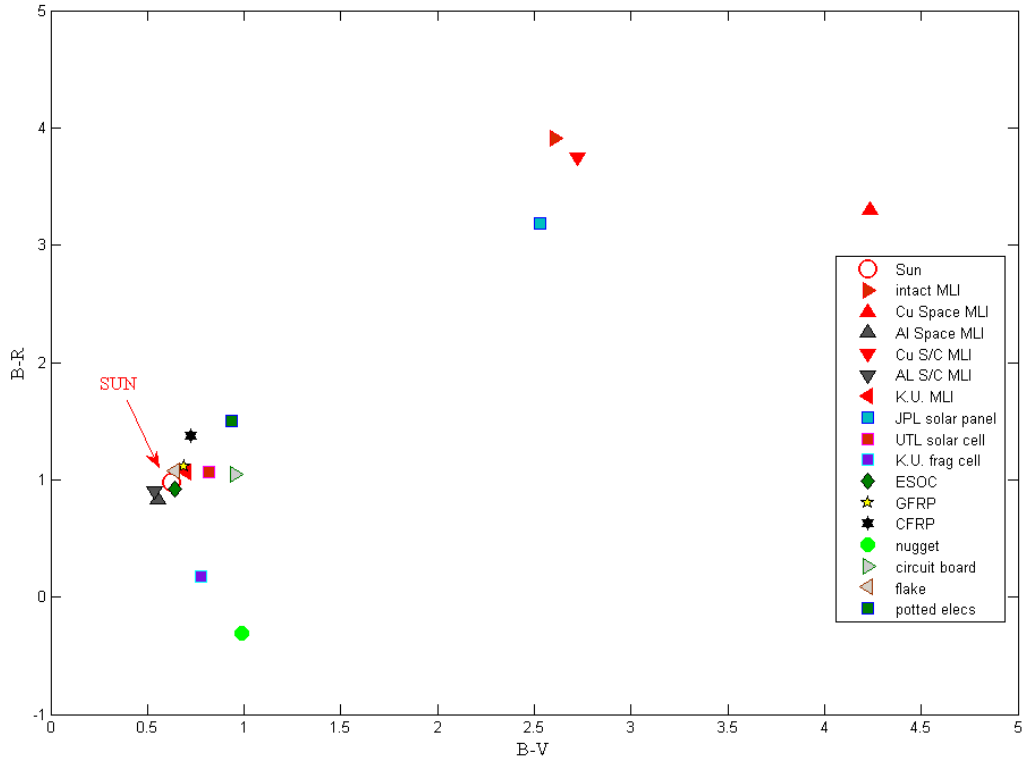


Fig. 1. Photometric B-R vs. B-V color indices for all 14 laboratory fragments.

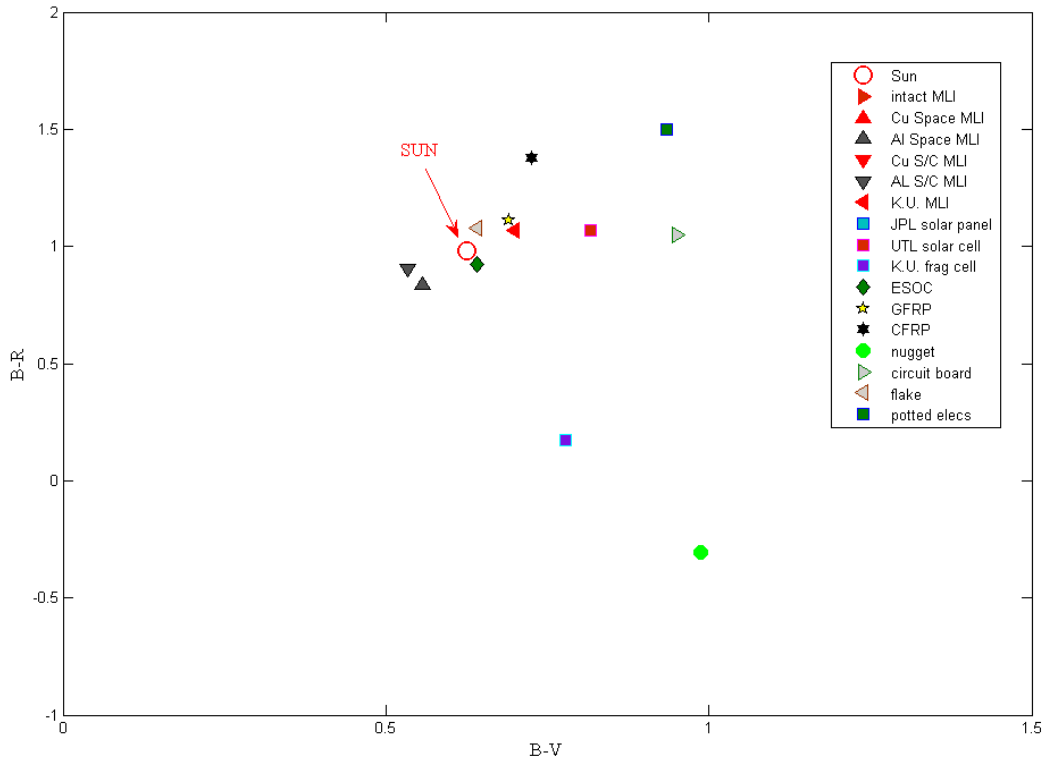


Fig. 2. Photometric B-R vs. B-V color indices for all 14 laboratory fragments, rescaled.

#### 4.2. Spectroscopic Average Color Indices

Spectral reflectance measurements possess a much higher wavelength resolution than photometric measurements. For example, when comparing the photometric data already presented, only one average value is calculated for each filter, whereas spectral measurements contain 250 measurements over the same bandpass. Spectral data was acquired using a subset of the pieces described earlier and several materials that were not measured using standard laboratory photometric techniques. Unlike the photometric samples; however, this laboratory spectral data will only show a diffuse reflectance (i.e., no specular components are included due to the equipment and software used) [2].

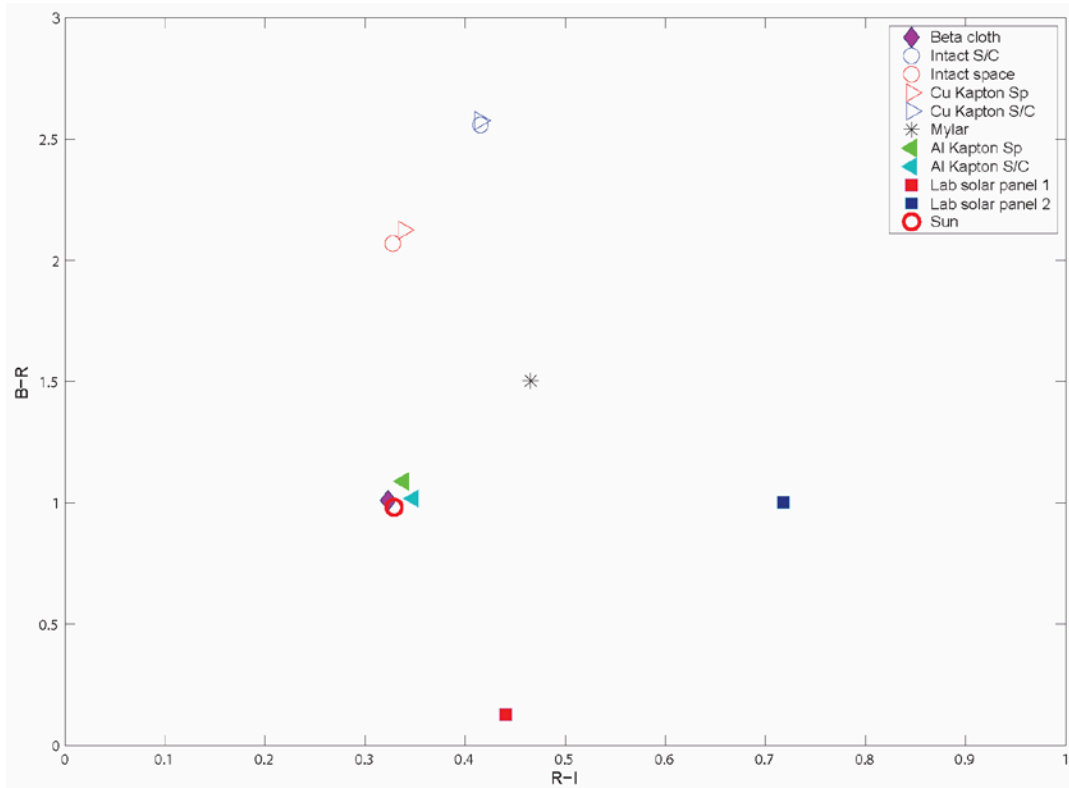


Fig. 3. Spectroscopic B-R vs. R-I color indices for selected laboratory samples.

As shown in Fig. 3, most objects measured using laboratory spectroscopy are “redder” than the solar value. The beta cloth and silver Kapton are both in close proximity to the solar value. The lab solar panel 1 (JPL sample composed of standard solar panel material with gallium arsenide solar cells) showed a higher signal in the infrared spectrum, but is closer to a blue response than any other material. The other laboratory solar panel sample is taken from a spacecraft and the details of the material type were not released.

When comparing these spectral measurements with the previous photometry measurements, the results showed the intact MLI to be far redder in the photometric data ( $B-R = 3.9 \pm 1.1$  vs.  $B-R = 2.6 \pm 0.1$  /  $2.1 \pm 0.1$  depending on the side). This could be a result of the specular components of the MLI, which as previously stated, cannot be measured with the spectrometer and/or the dilution of the primary surface reflectance by other areas illuminated in the photometry set-up. The two copper Kapton layers also had a higher reflectance in the red bandpass when using photometric techniques than when using spectral measurements, although the spectroscopic values were within the error variances of the photometric data. Using photographic measurements, the space-facing side showed a  $B-R = 3.3 \pm 1.3$  and the spacecraft-facing showed a  $B-R = 3.75 \pm 1.7$ , compared to a spectral measurement of  $B-R = 2.1 \pm 0.1$  and  $B-R = 2.6 \pm 0.1$ , respectively. Note that the differences between the two layer values (photometric and specular) are nearly equivalent: 0.45 and 0.5. The aluminized Kapton showed better agreement between the two sources, photometric  $B-R = 0.9 \pm 0.1$  and  $B-R = 0.8 \pm 0.2$  for the spacecraft- and space-facing layers respectively. The same layers exhibited a  $B-R = 1.0 \pm 0.2$  and  $1.0 \pm 0.4$  using spectral measurements, which are equivalent to the photometry data. The solar cells used in spectral measurements were localized to a specific area (solar cell material), unlike the photometric data that was collected using integrated values for all illuminated surfaces; therefore, the color indices

between the two measurement techniques are not expected to coincide greatly. The UTL solar cell had an integrated B-R of  $1.1\pm0.5$  and a spectral B-R of  $1.2\pm0.0$ , much closer in agreement than expected. The JPL solar panel had a composite of materials that would definitely affect the correlations between sources. The integrated B-R =  $3.2\pm0.3$  compared to the spectral B-R =  $0.1\pm0.1$  (which again only measured the solar cell material).

Spectral and photometric characteristics can vary depending on manufacture and mission, so the color-index data presented could have a broader range with a larger subset of similar materials. Also, spectral data are concentrated on one single material over a small surface area, whereas photometry is an integrated intensity value from all illuminated materials. The spectral data are collected to average over different areas, but may be very difficult for specular materials (e.g., Kapton and Mylar) that can easily saturate the detector. These data are used in the laboratory as a means of “truth” for the material color indices and to test the validity of the photometric equipment, but are not an absolute for comparison. The photometric data, therefore, are a better comparison to telescopic data that measure the intensity of an object as a function of all illuminated and visible surfaces.

## 5. COMPARISON TO TELESCOPE MEASUREMENTS

The Cerro Tololo Inter-American Observatory (CTIO) 0.9-m telescope, which is operated under the Small- and Medium-Aperture Research Telescope System (SMARTS) consortium, is located inland from La Serena, Chile and is used to acquire photometric measurements for the NASA Orbital Debris Program Office. The data are acquired through standard Johnson/Bessell B, V, R, and I filters. The data shown in Fig. 4 and Fig. 5 are identical to the laboratory data shown in Fig. 3, but with two types of GEO objects also plotted: stable (not varying magnitude over time) and flasher (large variations in magnitude over a short period of time). Both of these objects are uncorrelated targets, not catalogued by the U. S. Space Surveillance Network. The stable object (70509) data was taken over a 4-day time period (DOY 300, 300, 302, 303, 303, and 304), and the flasher (70511) data was acquired over 3 days (DOY 301, 303, 303, and 304), both of which had multiple acquisitions on specific nights. Note: The five-digit identification numbers associated with the objects are in-house numbers used for bookkeeping, not catalogued digits. The last two digits refer to object number tracked (i.e., the fifth or eleventh object tracked for a particular night) and the middle two digits refer to the observation run (i.e., ‘05’ was the fifth observation run corresponding to data taken in October of 2008). Although the OMC data presented have been corrected for solar illumination conditions, adjusting for space weathering effects is not currently possible at this time. Space weathering affects materials differently, white beta cloth tends to yellow and copper Kapton tends to redden, but applying a global space-weathering factor will take more time and research.

Based on color index data, the stable object appears to be in close proximity to the Mylar and laboratory solar panel. To make the best possible correlations between laboratory and remote data, the approximate A/m for objects in Earth orbit is required to narrow down the possible material correlations. For example, if the A/m of the GEO object presented in Fig. 4 was known, one could identify which material the object was best correlated to. With an A/m ratio between  $\sim 0.5 \text{ m}^2/\text{kg} < A/m < 1.0 \text{ m}^2/\text{kg}$ , the object best matches solar panel, while with an A/m exceeding  $30 \text{ m}^2/\text{kg}$ , the object likely is Mylar. Calculating the A/m for objects in orbit uses an interpreted result with several assumptions regarding the reaction of the surface to solar radiation pressure.

When comparing the laboratory data to telescope data, it was found that objects that are not stable, or objects with magnitudes that vary over half a magnitude or more, are impossible to correlate using color index plots due to the scatter in magnitude. The object shown in Fig. 5 is defined as a flasher, with high variations in magnitude over a short period or “glinting”. Even with the error variances included (largest value =  $\pm 0.3$ ), the magnitude scatter in the B-R and R-I color index plot (Fig. 5) makes correlations to laboratory data impractical. MLI and solar cell fragments are two common materials known to glint, thus making correlations to such materials more tedious. Although the object’s material cannot be determined, it is probable the material is highly reflective.

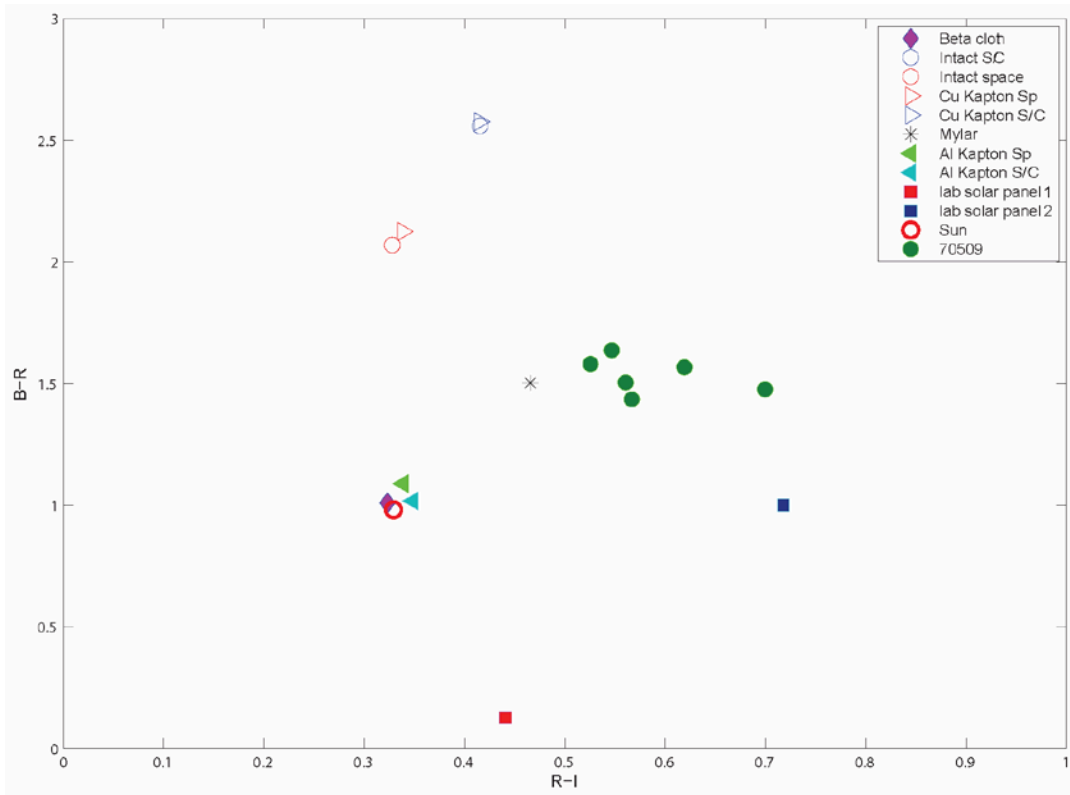


Fig. 4. Spectroscopic color indices with stable GEO object (70509).

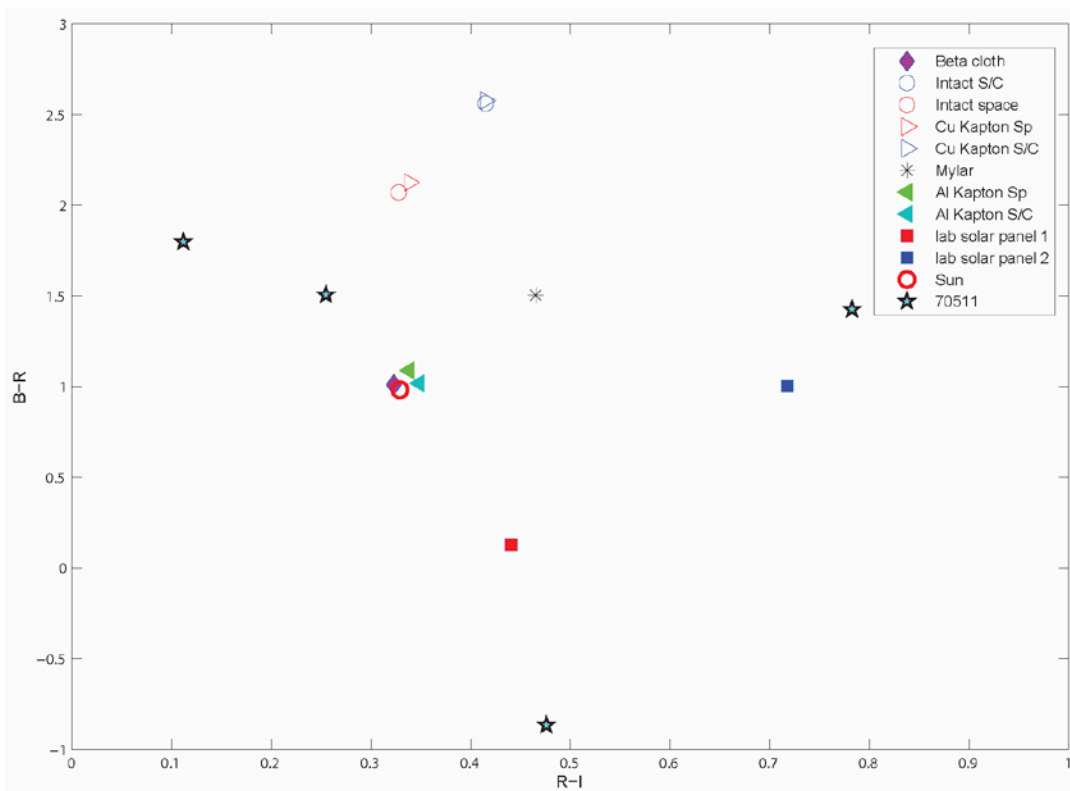


Fig. 5. Spectroscopic color indices with GEO "flasher" (70511).

Filter photometry data of another uncorrelated target (70513), is shown in Fig. 6. The filter photometry was taken using the CTIO 0.9-m telescope in the following sequence: R:B:I:V:R, always starting and finishing the sequence with the red filter to investigate any systematic change over the (~20 minutes) of the entire observation set. The initial R measurement is shown in red and the last R measurement is shown in purple. Data points contaminated by star streaks were removed. This object shows very small magnitude and color variations for short time scales (5 - 20 minutes), suggesting we are viewing just one aspect of this piece of debris. However, on longer timescales, both magnitude and colors change significantly (note the behavior near 3 hours UT), when the object brightens in B and V by approximately two magnitudes, yet becomes fainter in I by about the same amount. Shortly after 3 UT the object also becomes fainter in R by one and one-half magnitudes. The average B-R for each observation sequence began at 1.90 and ended with 1.63 nearly 3 hours later, but at 3 UT the B-R was approximately -0.23. This type of behavior is also seen in the OMC, when the MLI layer of copper-colored Kapton rotates toward the aluminized Kapton face. The magnitude changes from peaking in the R to peaking in the B or V, respectively, shown in Fig. 7 and Fig. 8. The B-R values do not match the telescope observational data at each orientation point, but the nature of the increase/decrease in magnitude for each respective filter is comparable.

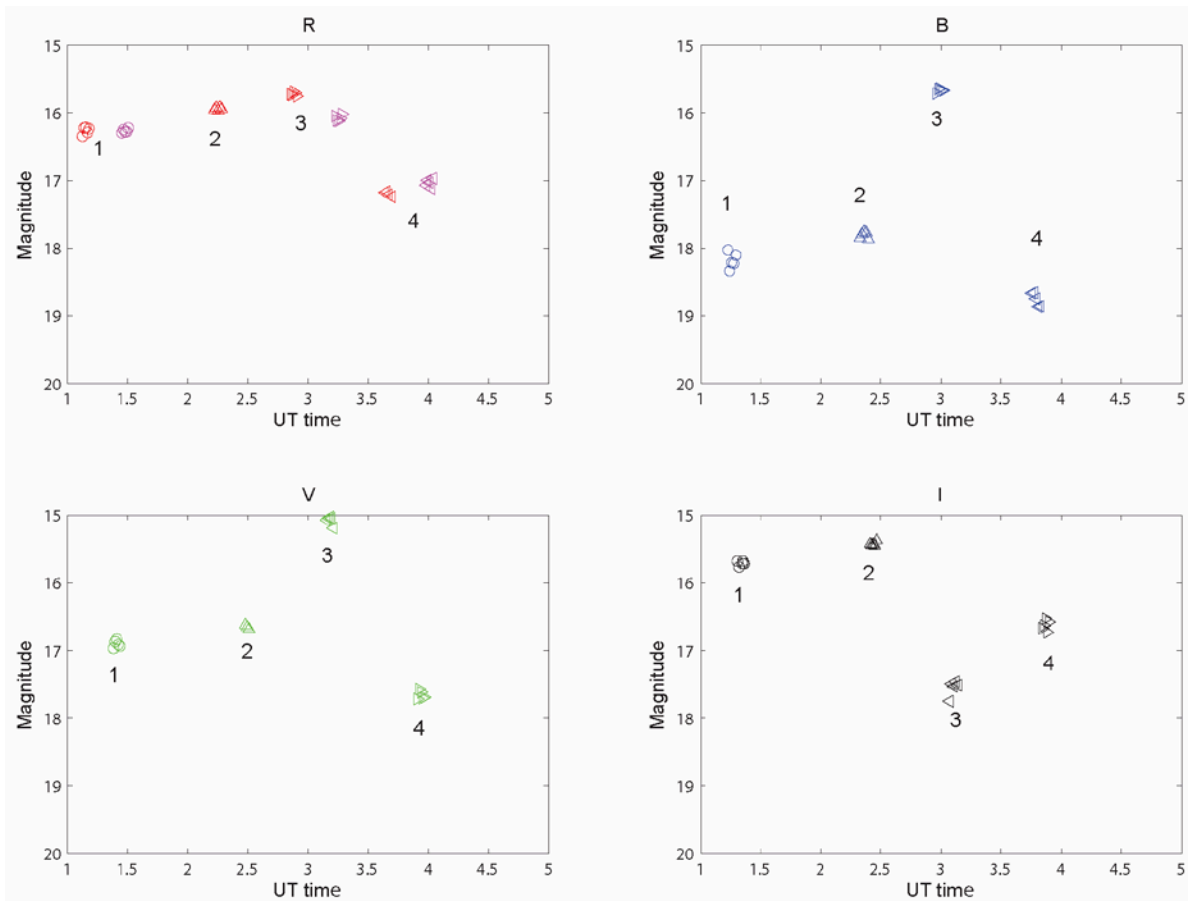


Fig. 6. Four sequences of filter photometry acquired by the CTIO 0.9-m on GEO object (70513).

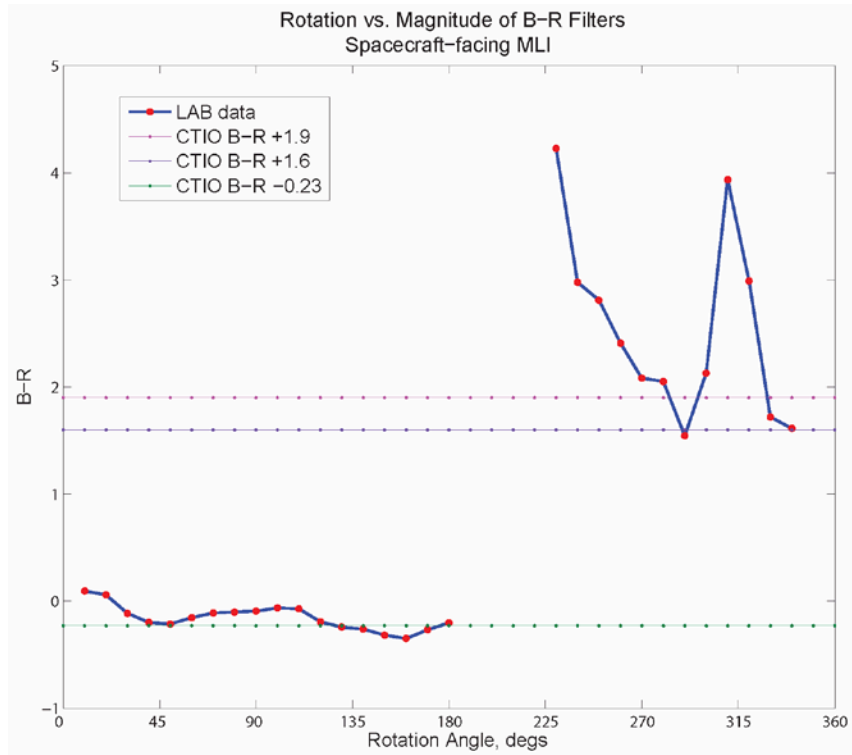


Fig. 7. B-R over a 360° rotation for space-facing MLI (copper-colored Kapton illuminated first, followed by aluminized Kapton) overlotted with telescopic B-R.

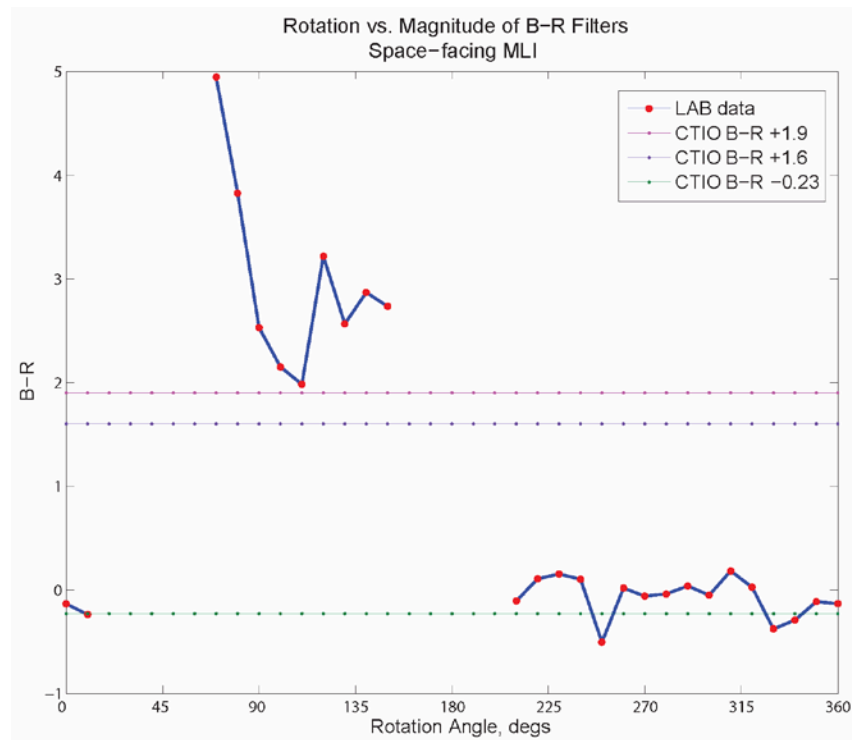


Fig. 8. B-R over a 360° rotation for spacecraft-facing MLI (aluminized Kapton illuminated first, followed by copper-colored Kapton) overlotted with telescopic B-R.

Data published from the European Space Agency (ESA) 1-m telescope of the Astronomical Institute of the University of Bern, was used as a secondary comparison for laboratory data. The ESA data provided lightcurves for various objects measured at different times, as well as estimated A/m values for observed objects. The comparisons between laboratory and ESA telescope data were based on A/m values, magnitude variations, and lightcurve characteristic structure. One specific set of data provided by the ESA 1-m telescope, taken at two different time periods, showed lightcurves of the same object, with an  $A/m = 1.9 \text{ m}^2/\text{kg}$ , with remarkably different lightcurve structures. Based on the calculated A/m for the laboratory MLI-intact sample and solar cell fragment, the ESA telescopic data would likely best match one of these samples. Unfortunately, without observations in multiple filters needed to define color indices, it was difficult to discriminate between the two possible laboratory materials [1].

## 6. CONCLUSIONS AND FUTURE WORK

Filter photometry was performed on a subset of 14 fragments collected from numerous possible sources of orbital debris, including destructive hypervelocity testing, pressure explosions, and flight-ready samples from possible spacecraft. These objects were chosen to best represent what one might expect for orbital debris, based on known materials, shapes, and sizes. The color index relative to the blue filter (B-V, B-R, and B-I) was presented for all objects with the exception of 4 objects which exhibited little to no signal in the *I* band and were not shown the B-I color index. Due to the material's low signal return in the *I* band, future measurements will increase the exposures (without saturation) and co-add more images to bring up SNR to help eliminate this issue. The B-R values showed good agreement between the spectral and photometric data. The majority of the color indices for the 14 fragments were near solar colors, whereas the copper Kapton materials showed magnitudes much redder than the sun. The JPL solar panel also showed close proximity to the copper Kapton material in the photometric color index plots, unlike the spectral data, which only concentrated on the solar cell material and was found to be much bluer than the sun.

Due to limited telescopic data, only several correlations could be presented. It was found that correlations to telescopic data must focus on stable objects; otherwise the magnitude scatter due to flashers/glints makes correlations impossible. One of the stable objects investigated showed a close proximity to Mylar and solar panel, but with two caveats: laboratory space weathering currently cannot be applied and without A/m values, the range of correlation possibilities cannot be minimized. Another object investigated using the CTIO 0.9-m appeared to be stable during each 5-minute sequence, but over a 2-hour period showed a dramatic magnitude change, increasing signal in the *B* and *V* filter, but decreasing shortly after in the *R* and *I* filters. This type of color change was consistent with laboratory measurements of the MLI layers when the aluminized Kapton layers are illuminated.

Future work will include increasing the number of fragments, material type, and shapes investigated, as well as extending the size range in an effort to develop an optical-based, size estimation model. A laboratory-based albedo distribution for multiple objects at different phase angles will also be acquired in future research. The current global albedo for all altitude ranges may not be sufficient for all materials and will be investigated. An improved albedo will lead to better definitions of debris sizes for optical measurements in the GEO regime.

## 7. REFERENCES

1. Cowardin, H., et al, An Assessment of GEO Orbital Debris Photometric Properties Derived from Laboratory-Based Measurements, 2009 AMOS Technical Conference Proceedings, Kihei, Maui, HI, 2009.
2. Cowardin, H., *Characterization of Orbital Debris Objects over Optical Wavelengths via Laboratory Measurements*, PhD thesis, Houston, TX, May 2010.
3. Hill, N., Measurement Techniques for Hypervelocity Impact Test Fragments, 59<sup>th</sup> International Astronautical Congress, September-October 2008, Glasgow, Scotland.
4. Reynolds, R.C., et al., NASA Standard Breakup Model 1998 Revision, September 1998.
5. Schildknecht, T., et al, Properties of High Area-to-Mass Ratio Space Debris Population in GEO, 2005 AMOS Technical Conference Proceedings, Kihei, Maui, HI, 2005.
6. Krisko, P., et al, SOCIT4 Collisional-Breakup Test Data Analysis: With Shape and Materials Characterization, *Advances in Space Research*, Volume 41, 2008.
7. Hanada, T. and Liou, J.C., Comparison of fragments by low- and hyper- velocity impacts, *Advances in Space Research*, Vol. 41, 1132-1137, 2008.
8. Fucke, W., and Sdunnus, H., Population Model of Small Size Space Debris, Final Report, ESOC # 9266/90/D/MD, Battelle-Institut, Frankfurt, Germany, April 1993.